Extending the host range of Listeria monocytogenes by rational protein design

Cell

Extending the Host Range of *Listeria monocytogenes* by Rational Protein Design

Thomas Wollert,[1] Bastian Pasche,[2] Maike Rochon,[3] Stefanie Deppenmeier,[4] Joop van den Heuvel,[3] Achim D. Gruber,[4] Dirk W. Heinz,[3] Andreas Lengeling,[2,*] and Wolf-Dieter Schubert[1,*]
[1] Molecular Host-Pathogen Interactions, Division of Structural Biology
[2] Infection Genetics, Department of Experimental Mouse Genetics
[3] Division of Structural Biology
Helmholtz Centre for Infection Research, Inhoffenstr. 7, D-38124 Braunschweig, Germany
[4] Department of Veterinary Pathology, Free University of Berlin, Robert-von-Ostertag-Str. 15, D-14163, Berlin, Germany
*Correspondence: wolf-dieter.schubert@helmholtz-hzi.de (W.-D.S.), andreas.lengeling@helmholtz-hzi.de (A.L.)
DOI 10.1016/j.cell.2007.03.049

SUMMARY

In causing disease, pathogens outmaneuver host defenses through a dedicated arsenal of virulence determinants that specifically bind or modify individual host molecules. This dedication limits the intruder to a defined range of hosts. Newly emerging diseases mostly involve existing pathogens whose arsenal has been altered to allow them to infect previously inaccessible hosts. We have emulated this chance occurrence by extending the host range accessible to the human pathogen *Listeria monocytogenes* by the intestinal route to include the mouse. Analyzing the recognition complex of the listerial invasion protein InlA and its human receptor E-cadherin, we postulated and verified amino acid substitutions in InlA to increase its affinity for E-cadherin. Two single substitutions increase binding affinity by four orders of magnitude and extend binding specificity to include formerly incompatible murine E-cadherin. By rationally adapting a single protein, we thus create a versatile murine model of human listeriosis.

INTRODUCTION

The constant interaction of humans with countless microorganisms has led to the evolution of an intricate, multifaceted, and remarkably efficient immune system. Pathogens have, however, coevolved, refining their arsenal of pathogenicity factors to exploit loop holes in the host's defenses (Akira et al., 2006). This dedicated specialization of pathogens restricts their choice of alternative hosts and limits the usefulness of animal models to study human pathogens in vivo. Molecular mechanisms defining host tropism have been identified for a limited number of pathogens, including the food-borne human pathogen *Listeria monocytogenes* (Hamon et al., 2006). These include two listerial invasion proteins, internalin (InlA) and InlB, that promote uptake of bacteria into distinct sets of nonphagocytotic cells (Cossart et al., 2003).

InlA promotes listerial uptake into intestinal epithelial cells (Gaillard et al., 1991) by targeting the N-terminal domain of human E-cadherin (hEC1) (Mengaud et al., 1996), the dominant adhesion molecule of adherens junctions (D'Souza-Schorey, 2005). InlA similarly recognizes E-cadherin from guinea pig and rabbit but fails to bind the corresponding domain of murine E-cadherin (mEC1), despite a sequence identity of 90% to hEC1 (Lecuit et al., 1999) and a pronounced structural similarity (Schubert et al., 2002). Among other targets, the second listerial invasion protein InlB recognizes the HGF or Met receptor (Shen et al., 2000) inducing uptake into a wide range of mammalian cells including hepatocytes and endothelial cells. InlB recognizes both murine and human Met receptor but not that of the guinea pig and rabbit (Khelef et al., 2006). The lack of a small-animal model to study the interplay of InlA and InlB in human listeriosis in vivo was first addressed by the generation of a transgenic mouse producing human alongside murine E-cadherin in its enterocytes (Lecuit et al., 2001), thereby allowing the role of InlA and of other virulence factors to be characterized in orally infected mice (Sabet et al., 2005; Khelef et al., 2006; Boneca et al., 2007).

Animal models for other pathogens have similarly been created by the genetic humanization of mice (Lecuit and Cossart, 2002). However, because pathogens typically abuse host molecules of complex biological function, humanizing such molecules may incur unexpected secondary effects. Humanized mouse lines, furthermore, need to be crossed with existing knockout strains (Yap and Sher, 2002), thereby adding another level of complexity.

In nature, pathogens occasionally switch their host specificity through spontaneous changes in their molecular arsenal (Gamblin et al., 2004), causing in high mortality

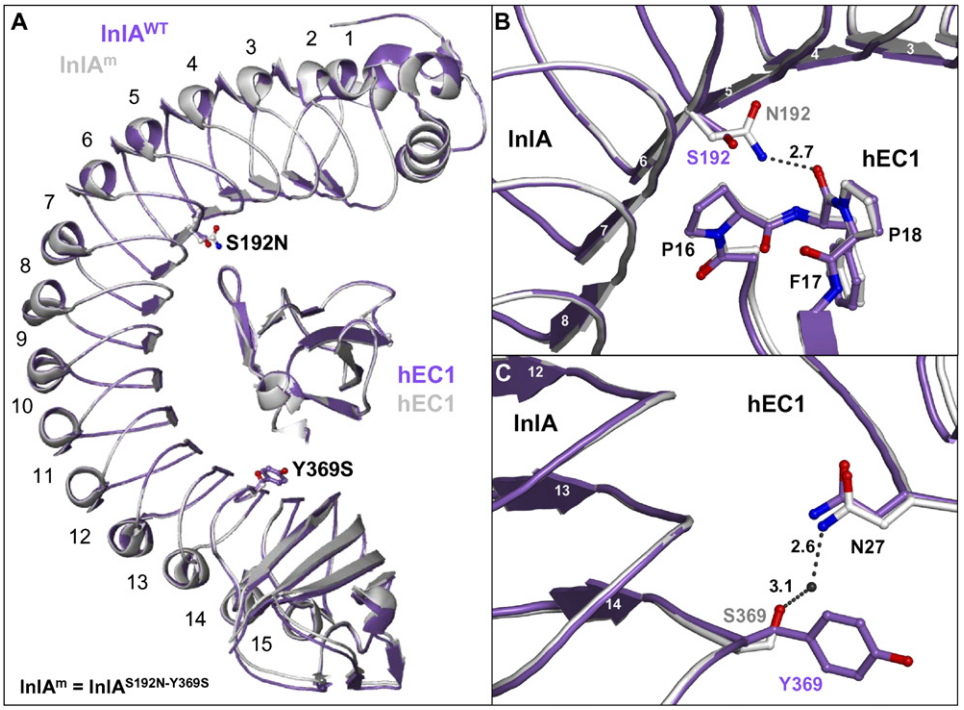

Figure 1. Re-engineered Variants of Internalin (InlA) in Complex with the N-Terminal Domain of Human E-Cadherin

(A) Superposition of InlA/hEC1 (violet) and $InlA^{S192N-Y369S}$/hEC1 (gray).

(B) Critical residues near mutation site $S192N_{InlA}$ are shown as ball and stick. $Asn192_{InlA}$ adds a direct H bond to the carbonyl oxygen of $Phe17_{hEC1}$.

(C) The mutation $Y369S_{InlA}$ introduces a water-bridged interaction to $Asn27_{hEC1}$.

rates in the naive host population (Weiss, 2003). Zoonotic pathogens eliciting recent pandemics in the global human population (Lewis, 2006) include HIV (Heeney et al., 2006) and SARS (Li et al., 2005), whereas influenza A subtype H5N1 may be poised to do the same (Stevens et al., 2006).

We imitate this natural route of pathogen evolution by extending the host spectrum of *Listeria monocytogenes*. Our approach is based on the rational structure-based re-engineering of InlA such that modified InlA is able to recognize the previously incompatible receptor mEC1. By adapting the bacterium to the mouse ("murinization") rather than humanizing the mouse, we introduce the human route of infection in mice and hence provide a versatile animal model to investigate listeriosis in vivo.

RESULTS

Structure-Based Virulence-Factor Design

Our working hypothesis was that the weak binding affinity of InlA for hEC1 is due to imperfect surface complementarity and hence numerous bridging water molecules between the two proteins (Schubert et al., 2002). To increase binding affinity, we proposed individual amino acid substitutions in InlA (Figure 1A) to create additional, stabilizing contacts to hEC1, thus improving complementarity and binding affinity.

Although Ser192 of InlA ($Ser192_{InlA}$) faces hEC1 in the complex InlA/hEC1, its side chain is too short for a direct hydrogen bond to hEC1. Replacing it by asparagine could allow such a direct interaction. Solving the crystal structure of $InlA^{S192N}$/hEC1 confirms that engineered $Asn192_{InlA}$ creates a direct hydrogen bond to the main-chain carbonyl of $Phe17_{hEC1}$ (Figure 1B). Correspondingly, isothermal titration calorimetry (ITC) indicates the dissociation constant (K_D) of $InlA^{S192N}$/hEC1 to be 200 ± 50 nM (Figure 2), a 40-fold increase in binding affinity relative to $InlA^{WT}$/hEC1 (K_D = 8 ± 4 μM).

To improve the unfavorable interaction of bulky $Tyr369_{InlA}$ to hEC1, we chose to replace it by the small hydrophilic amino acid serine. The crystal structure of the double variant $InlA^{S192N-Y369S}$ (henceforth denoted $InlA^m$) in complex with hEC1 confirms that the interaction of $Tyr369_{InlA}$ has been replaced by a water-mediated hydrogen bond from $Ser369_{InlA}$ to $Asn27_{hEC1}$ (Figure 1C). The binding affinity of $InlA^m$ for hEC1 is found to be K_D = 1.2 ± 0.3 nM by ITC. The substitution $Y369S_{InlA}$ thus increases binding affinity by a factor of 170 (Figure 2), whereas both substitutions together increase affinity 6700-fold compared to $InlA^{WT}$/hEC1. Although separated by 34 Å, the substitutions convert a weak interaction to a tight recognition. Note that a mere eight nonhydrogen atoms within the recognition interface of InlA and hEC1 have been altered.

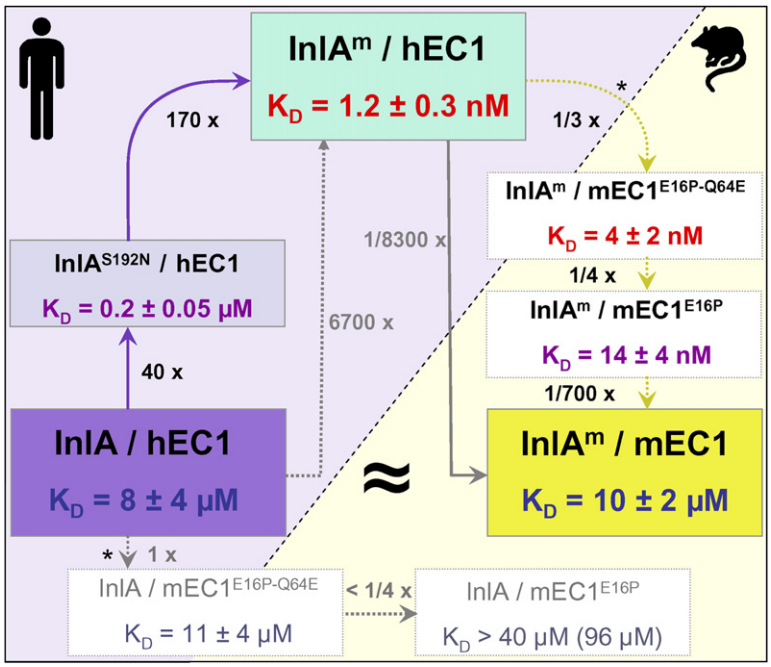

Figure 2. Re-engineering the Interaction of InlA and E-Cadherin

Colored boxes represent protein complexes and their dissociation constants (K_D). Shades of violet to cyan indicate complexes involving human E-cadherin (hEC1), whereas shades of yellow and white complexes indicate complexes involving murine E-cadherin (mEC1). Two substitutions in InlA generate $InlA^{S192N}$ and $InlA^{S192N-Y369S}$ ($InlA^m$). Binding affinity for hEC1 increases 40- and 170-fold (together 6700-fold). The eleven substitutions separating hEC1 and mEC1 reduce binding affinity of $InlA^m$ 8300-fold. Coincidentally, binding affinities of InlA/hEC1 (dark violet) and $InlA^m$/mEC1 (yellow) are essentially identical. The affinity of $InlA^m$ and $InlA^{WT}$ for $mEC1^{E16P}$ is significantly lower than for hEC1. Doubly substituted $mEC1^{E16P-Q64E}$ is recognized with similar affinity as hEC1, indicating improved humanization of mEC1 (white boxes). The asterisks indicate nine substitutions that separate hEC1 from $mEC1^{E16P-Q64E}$.

Effect of Improved Affinity in Human Cells

To analyze the biological effects of improved affinity of $InlA^m$ on the adhesion to and invasion of human epithelial cells in vitro, we modified wild-type *Listeria monocytogenes* EGD (Lmo-EGD) by exclusively replacing the gene *inlA* by $inlA^{S192N-Y369S}$ to produce the mutant strain Lmo-$InlA^m$. Our strategy of minimal intervention circumvents InlA and InlB expression-level changes caused by disrupting the bicistronically transcribed *inlAB* locus (Lingnau et al., 1995). Both listerial invasion proteins are thus expressed at native levels, ensuring that valid biological conclusions may be drawn from the infection process (Figure S1 in the Supplemental Data available online).

Binding of InlA to human E-cadherin induces listerial uptake into human epithelial cells by the zipper mechanism (Cossart and Sansonetti, 2004), requiring localized rearrangements of the cytoskeleton as well as a physically tight interaction between bacterium and eukaryotic cell membrane. To establish whether improved affinity of $InlA^m$ for its receptor results in stronger adhesion of Lmo-$InlA^m$, we analyzed its adhesion to the E-cadherin expressing human epithelial cell line Caco2. We observe a 2-fold increase in the adhesion efficiency of Lmo-$InlA^m$ compared to wild-type bacteria (Figure 3A).

We investigated the link between improved adhesion of Lmo-$InlA^m$ and bacterial uptake by using

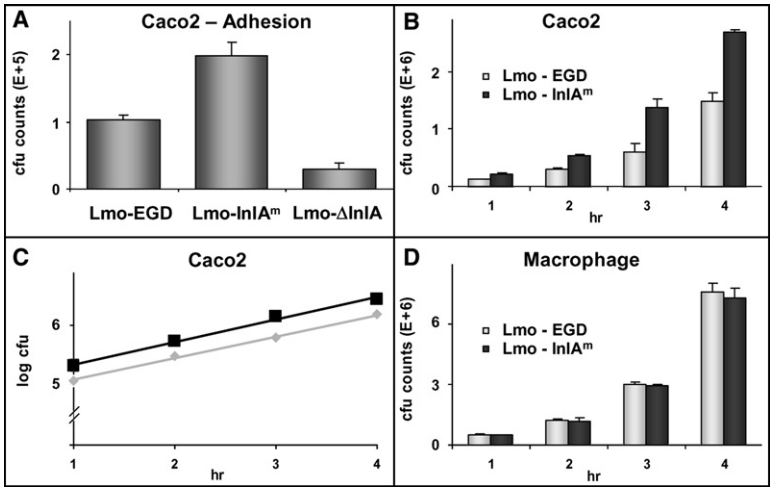

Figure 3. Adhesion and Intracellular Growth of Lmo-EGD and Lmo-$InlA^m$

(A) Adhesion assay. Confluent layers of Caco2 cells were infected with Lmo-EGD, Lmo-ΔInlA, or Lmo-$InlA^m$ for 30 min. Cells were washed extensively, and lysates were plated onto BHI agar plates.

(B and C) Intracellular growth curve of Lmo-EGD and Lmo-$InlA^m$ in Caco2 cells. Extracellular bacteria were killed after 1 hr by gentamicin. We quantified intracellular bacteria after 1–4 hr by plating cell lysates onto BHI agar plates. (B) shows observed cfu-values. (C) shows that the mean bacterial doubling time is 50 ± 4 min (gradient of the linear log cfu plotted against time).

(D) Intracellular growth curve of Lmo-EGD and Lmo-$InlA^m$ in the macrophage-like cell line J774 where uptake is InlA independent. Cells were infected for 30 min, and intracellular bacteria were quantified after 1–4 hr. All observed cfu values were corrected for differences in the starting inoculum. Data show one representative of three independently performed experiments.

Gentamicin-protection-invasion assays (Elsinghorst, 1994). We observe a doubling in the number of internalized bacteria when expressing InlA^{m} compared to InlA^{WT} (Figure 3B). Increased invasion thus appears to be predominantly caused by improved adhesion of Lmo-InlA^{m} to Caco2 over Lmo-EGD.

After phagocytosis, bacteria need to escape from the phagosome to avoid lysosomal degradation. To rule out that factors after uptake affect the observed increase in intracellular bacteria, we analyzed intracellular growth rates of Lmo-EGD and Lmo-InlA^{m}. A plot of colony-forming units (cfu) against time (Figure 3B) indicates a similar exponential increase for both Lmo-EGD and Lmo-InlA^{m}. A logarithmic plot (Figure 3C) reveals the replication time of both strains to be 50 ± 4 min (gradient). The re-engineering of InlA therefore predominantly affects the process of listerial adhesion, whereas uptake, phagosomal escape, intracellular replication rates, and cell-to-cell spread appear unaltered.

As a control, we compared intracellular growth curves of both strains in the professionally phagocytic, macrophage-like cell line J774, where uptake is InlA independent (Dramsi et al., 1997). We observe indistinguishable invasion efficiencies and intracellular replication times of 46 ± 3 min for both strains (Figure 3D). InlA-independent pathophysiological characteristics of Lmo-EGD thus remain unaltered in Lmo-InlA^{m}.

Modifying Binding Specificity

Although E-cadherin and in particular the N-terminal domain EC1 is highly conserved among mammals, the differences in amino acid sequence vary sufficiently to disallow binding of InlA to murine EC1 (mEC1). As a consequence, E-cadherin-based invasion of murine epithelial cells does not occur (Lecuit et al., 1999).

We find the dissociation constant of InlA^{m}/mEC1 to be K_D = 10 ± 2 μM (Figure 2). Although weak, the binding affinity almost perfectly matches the K_D = 8 ± 4 μM for InlA^{WT}/hEC1 (Schubert et al., 2002). The high-resolution crystal structure of InlA^{m}/mEC1 (Figures 4B–4D and Table S1) indicates that the relative orientations of mEC1 and InlA^{m} are unchanged from InlA/hEC1 (r.m.s.d. for main-chain atoms ~0.7 Å). The hydrogen bonds introduced to strengthen the interaction of InlA/hEC1 (see above) are retained in InlA^{m}/mEC1, thereby giving rise to the altered specificity of InlA.

Differences between InlA/hEC1 and InlA^{m}/mEC1 most noticeably involve residues 16 of hEC1 and mEC1 and their immediate neighborhood. Pro16$_{hEC1}$ adopts a strained *cis* conformation, optimally positioning its side chain within a hydrophobic binding pocket of InlA (Figure 4C). Glu16$_{mEC1}$ of the engineered complex, by contrast, adopts a relaxed *trans* conformation, permitting the backbone to move aside to accommodate the longer glutamate side chain. Unexpectedly, the carboxy group of Glu16$_{mEC1}$ occupies the same hydrophobic pocket of InlA as Pro16$_{hEC1}$ in InlA/hEC1 (Figure 4C). Glu16$_{mEC1}$ additionally induces a local rearrangement that involves Lys19$_{mEC1}$ and that repositions the latter away from a salt bridge to Glu255$_{InlA}$ observed in InlA/hEC1 (Schubert et al., 2002). The low binding affinity of InlA for mEC1 is thus not only due to the disparate physical properties of glutamate and proline but also due to local adjustments within EC1 (Figure 4D).

A Second Determinant of Binding Affinity

The substitution of Pro16$_{hEC1}$ by Glu16$_{mEC1}$ clearly dominates the host tropism of *L. monocytogenes* (Lecuit et al., 1999). Genetically replacing Glu16$_{mEC1}$ by proline in mice has been proposed as a route to create a new animal model, rendering all E-cadherin expressing cells susceptible to InlA-mediated entry (Lecuit, 2005). Analyzing the affinity of InlA for mEC1^{E16P} biophysically, we find the interaction to be exceedingly weak (K_D > 40 μM), preventing the binding affinity from being quantified unambiguously. We estimate the binding affinity as follows: InlA^{m} binds mEC1^{E16P} with a K_D = 14 ± 4 nM (Figure 2) and thus confirms the dominant effect (factor of 700) of the Glu16Pro substitution. The ten remaining substitutions in mEC1 (Figure 4A) contribute a factor of ~12 (Figure 2). Provided the changes are largely additive, the K_D of InlA/mEC1^{E16P} would be ~12 × K_D = 8 μM (InlA/hEC1) or ~96 μM (Figure 2). In InlA-coated latex beads, this low binding affinity could be offset by a high density of InlA molecules leading to recognition of mEC1^{P16E}-expressing cells (Lecuit et al., 1999). On the surface of *Listeria*, physical and physiological constraints would limit the density of InlA, preventing efficient adhesion and hence uptake of Lmo-EGD.

The crystal structure of InlA^{m}/mEC1 reveals that a second substitution in mEC1 is involved in InlA^{m} recognition. In InlA/hEC1, Glu64$_{hEC1}$ forms a salt bridge to Arg85$_{InlA}$ (Figures 4A and 4B). In mEC1, this glutamate is replaced by glutamine, substituting the salt bridge by a hydrogen bond to Arg85$_{InlA}$. Reverting these two substitutions in mEC1 produces mEC1$^{P16E-Q64E}$ with an affinity of K_D = 4 ± 2 nM for re-engineered InlA^{m} (Figure 2) or K_D = 11 ± 4 μM for InlA^{WT}—similar to that of InlA/hEC1 (K_D = 8μM). A transgenic mouse bearing both the substitutions Glu16-Pro and Gln64Glu in murine E-cadherin could therefore represent a system more closely resembling the human situation than the singly substituted protein.

Altered Host Tropism In Vivo

To establish whether increased binding affinity of InlA^{m} for murine E-cadherin will allow infection of the murine intestine comparable to that of humans, we infected C57BL/6J mice intragastrically with both Lmo-EGD and Lmo-InlA^{m}. Challenging mice with 5 × 10^{7} to 5 × 10^{10} Lmo-InlA^{m} results in dose-dependent mortality rates (Figure 5A). The median lethal dose is inferred to be ~5 × 10^{7}. By contrast, the highest achievable inoculum of 5 × 10^{10} of Lmo-EGD is lethal only for ~20% of infected mice (Figure 5A, dashed line). Lmo-InlA^{m} is thus at least three orders of magnitude more virulent in mice than wild-type Lmo-EGD.

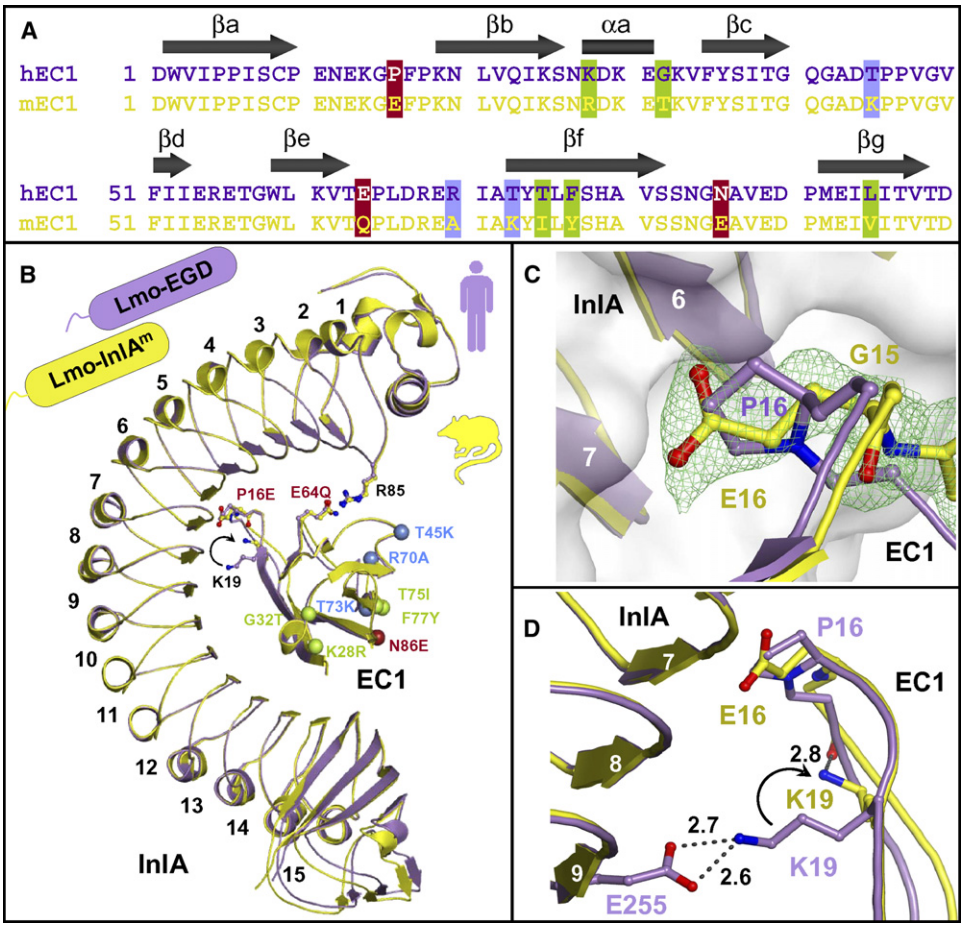

Figure 4. Comparison of InlA/hEC1 and InlA^m/mEC1 Complexes

(A) Sequence alignment of the N-terminal, extracellular domains (EC1) of human (hEC1, violet), and murine (mEC1, yellow) E-cadherin. Sequence differences involving charged residues are marked by red and blue boxes, and all others were marked by green boxes.

(B) Superposition of both protein complexes. LRRs are numbered. Critical residues are shown as ball and stick, and solvent-exposed substitutions are shown as spheres (colors are as shown in [A]).

(C) Hydrophobic Pro16$_{hEC1}$ (violet) is accommodated in a hydrophobic pocket of InlA. The carboxylate of Glu16$_{mEC1}$ (yellow), well defined in the $2F_O$-F_C difference electron density (green, contoured at 1σ), occupies the same pocket.

(D) Lys19$_{hEC1}$ forms a favorable salt bridge to InlA. *Trans* Glu16$_{mEC1}$ repositions Lys19$_{mEC1}$, trapping its side-chain through an intramolecular H-bond (arrow).

To establish the route of infection of Lmo-InlA^m in mice, we analyzed the load of Lmo-InlA^m and Lmo-EGD in affected organs, after intragastric challenge with 1×10^{10} bacteria (Figure 5 and Figure S2). In stomach and intestine, loads of Lmo-InlA^m and Lmo-EGD (Figures 5B and 5C) are largely comparable until day 2 post infection (p.i.). Thereafter, Lmo-InlA^m loads increase strongly (Figures 5B and 5C), whereas loads of Lmo-EGD remain constant.

In mesenteric lymph nodes, the spleen, and the liver, bacterial loads of both strains increase until day 2 p.i. (Figures 5D–5F). Lmo-EGD counts then stabilize in mesenteric lymph nodes, the spleen, and the liver (infection controlled). In Lmo-InlA^m-infected mice, by contrast, stabilization of bacterial numbers is not observed. Instead, bacterial loads increase exponentially in the spleen and liver until day 4 p.i. (solid lines, Figures 5E and 5F), resulting in 1.000-fold greater bacterial numbers in the spleen and liver in Lmo-InlA^m than in Lmo-EGD on day 4 p.i. Bacterial counts in mesenteric lymph nodes diverge after day 2 p.i., but loads of Lmo-InlA^m increase more slowly than in the liver and spleen.

To compare bacterial-growth kinetics at a lower infection dose, we challenged mice intragastrically with 5×10^7 of Lmo-EGD and Lmo-InlA^m (Figure S3). Again, we observe enhanced virulence for Lmo-InlA^m relative to Lmo-EGD. Although the effect in terms of bacterial numbers is not as pronounced as for the higher dose, slower kinetics of bacterial dissemination allow later time points to be investigated. In the stomach and small intestine, differences in bacterial loads become significant by day 5 p.i. In the

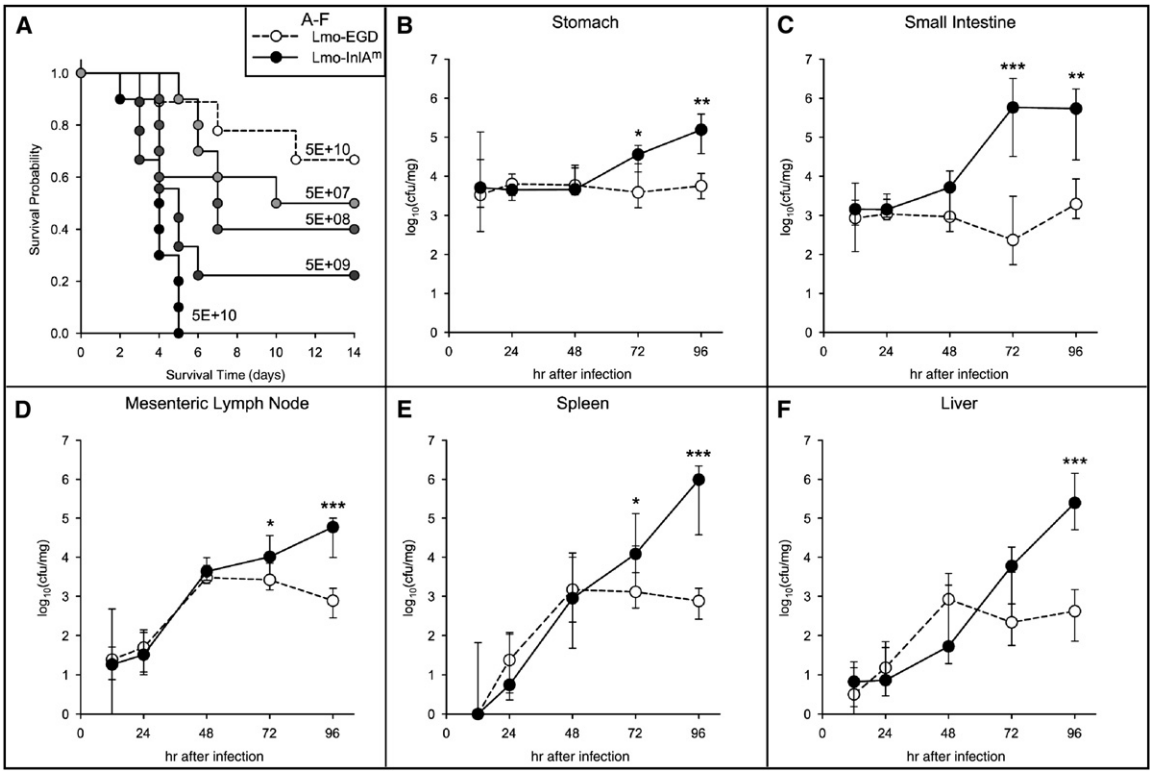

Figure 5. Survival of Mice Intragastrically Infected with Lmo-EGD and Lmo-InlA^m and Associated Bacterial Organ Loads over Time

Survival curves (A) and organ loads (B–F) of female C57BL/6J mice inoculated intragastrically with Lmo-EGD (dashed curve, ○) or Lmo-InlA^m (solid curves, ●). (A) shows that Lmo-InlA^m exhibit more than 1000-fold higher virulence than wild-type Lmo-EGD (inocula as indicated, n = 10 for each bacterial strain and experiment). (B–F) shows that 1×10^{10} bacteria of either strain were administered intragastrically to analyze kinetics of bacterial growth (n = 6 for 24 h p.i. and n = 12 for all others). Organ loads were ascertained at five time points in the stomach (B), small intestine (C), mesenteric lymph nodes (D), spleen (E), and liver (F). All data are from two independent experiments. The bar represents the median for each time point and genotype; 95% confidence intervals are indicated. Statistical significance by Mann-Whitney U nonparametric test: *$p < 0.05$, **$p < 0.01$, and ***$p < 0.001$.

spleen, liver, and mesenteric lymph nodes, Lmo-InlA^m loads are consistently higher than those of Lmo-EGD.

Histological Analysis of InlA-Dependent Infection Mechanisms

Histological and immunohistochemical studies of Peyer's patches of infected mice indicate that both Lmo-EGD and Lmo-InlA^m remain restricted to the dome and germinal centers, where they induce neutrophil infiltration and necrosis (Figures S4A–S4D) with gradually increasing severity along the small-intestinal axis. Colonization is, however, essentially indistinguishable until day 4 p.i. Whereas the Lmo-EGD infection subsides after day 4 p.i., no such remission is observed for Lmo-InlA^m.

Immunohistochemical analyses of the intestinal mucosa clearly demonstrate that Lmo-EGD do not invade epithelial tissue (Figure 6). Instead, bacteria are exclusively observed in the lumen or occasionally adhere to the surface of individual villi (Figures 6B, 6F, and 6J) as late as day 4 p.i. (Figure 6N). Similarly, the intestinal tissue is fully intact without any signs of inflammation until day 3 p.i. (Figures 6A and 6E). Transient inflammatory response with enhanced mucus secretion and mild, local erosion of epithelium is present at day 4 p.i. (Figure 6I). The inflammation, however, subsides by day 5 p.i. (Figure 6M).

In Lmo-InlA^m-infected mice, colonization of epithelia at villous tips are observed 24 hr p.i. in the ileum (Figure 6D), rapidly spreading to extended areas of the epithelium and accumulating within the lamina propria (subepithelial tissue) (Figures 6H, 6L, and 6P). On day 4 p.i., high bacterial loads cause erosion of the epithelium and fusion of villi (Figures 6K and 6O). Lesions are more pronounced in the ileum than in the duodenum and jejunum.

Role of InlA in Systemic Spread

To analyze the role of InlA^m in systemic infections of internal organs independently of intestinal uptake, we inoculated mice intravenously (i.v.) with both low (5×10^3) or high (2.4×10^4) doses of Lmo-EGD or Lmo-InlA^m. In contrast to the oral route of infection, the survival rates for both strains are found to be indistinguishable for both bacterial doses (Figures 7A and 7B). Similarly, bacterial loads in mesenteric lymph nodes, the spleen, and the liver at different time points after i.v. inoculation demonstrate

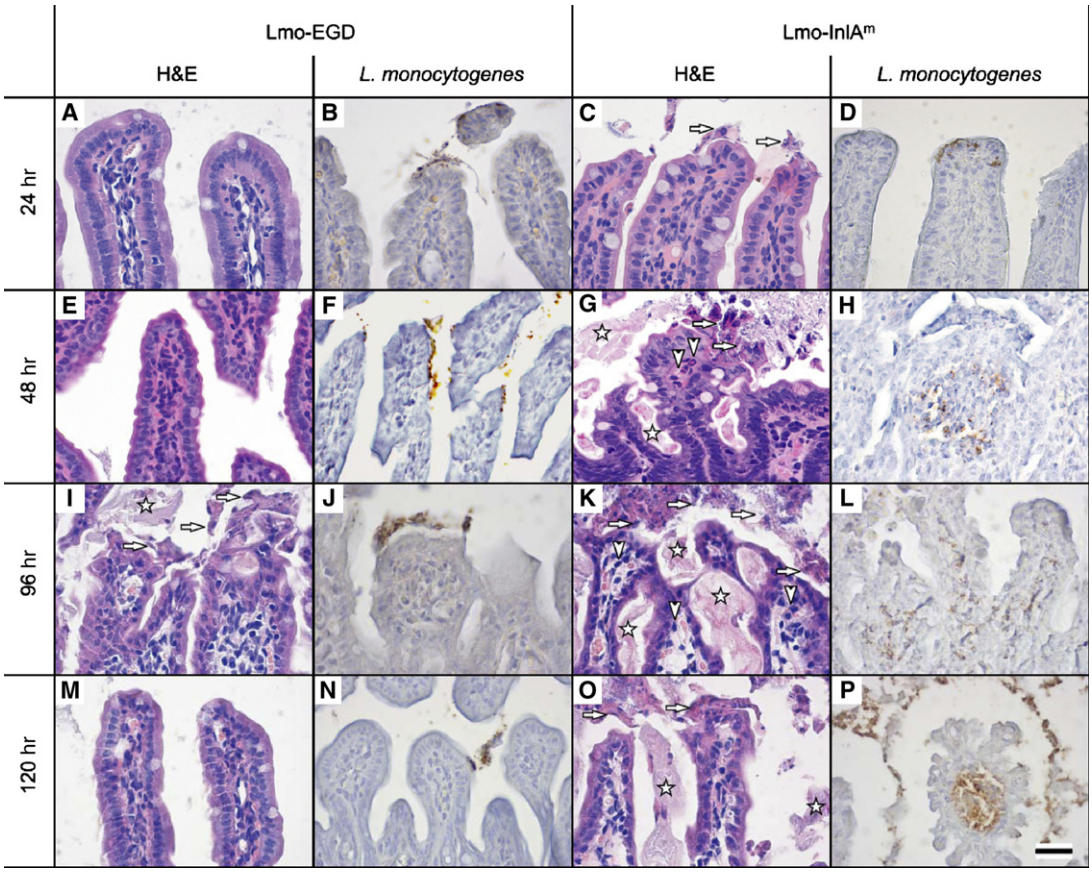

Figure 6. Comparing the Spread of Lmo-EGD and Lmo-InlA^m in the Small Intestine

Histology and immunohistochemical detection of *Listeria* in the distal part of the small intestine of C57BL/6J mice 24, 48, 96, and 120 hr after intragastric inoculation with 1.5×10^{10} Lmo-EGD or Lmo-InlA^m. The intestinal epithelium was analyzed by H&E staining or anti-*Listeria* immunohistochemistry. In Lmo-EGD-infected mice, no lesions and inflammatory responses are seen either (A) 24 or (E) 48 hr p.i. (I) shows that 96 hr p.i., moderate inflammation is visible with mild apical epithelial cell necrosis (horizontal arrows) and increased secretion of mucus (star). (M) demonstrates that 120 hr p.i., the intestinal epithelium is fully regenerated. This correlates with anti-*Listeria* staining, where Lmo-EGD are located in the intestinal lumen, occasionally associated with villi surfaces, without detectable invasion (B, F, J, and N). (C) and (D) show that 24 hr p.i., Lmo-InlA^m-infected mice reveal mild erosion of epithelial cells exclusively seen at tips of the villi (horizontal arrows). (G) and (K) show that 48 and 96 hr p.i., widespread necrosis, loss of villous epithelial cells (horizontal arrows), and massive secretion of mucus (indicated by stars) are clearly visible. Neutrophils and lymphocytes (vertical arrows) infiltrate the villi. (H) and (L) show that these observations coincide with extensive colonization of the epithelium and deeper tissues (lamina propria) of villi by Lmo-InlA^m. (O) shows that 120 hr p.i., necrotic enterocytes are shed into the intestinal lumen (horizontal arrows). Overproduction of mucus (stars) and distortion of villous structures are also apparent. (P) shows that this corresponds to extensive growth of Lmo-InlA^m in the epithelium and lamina propria. The scale bar (for all) represents 50 μm.

comparable virulence of Lmo-EGD and Lmo-InlA^m (Figures 7C–7E).

Blood-Placental Barrier

Lmo-EGD remains problematic to humans inter alia because of its ability to cross the blood-placental barrier, thereby resulting in sepsis or miscarriage. Ex vivo experiments have shown that InlA-mediated entry into human placental trophoblasts is important in placental infection (Lecuit et al., 2004). Studies of Lmo-EGD-infected pregnant BALB/c mice (functional InlB, nonfunctional InlA) (Le Monnier et al., 2007) and guinea pigs (functional InlA and nonfunctional InlB) (Bakardjiev et al., 2004) indicate that InlA and InlB individually are insufficient at inducing vertical transmission in vivo. They, however, confirm trophoblasts to be the primary target of Lmo-EGD. To ascertain whether the combination of functional InlA and InlB facilitates vertical transmission, we analyzed the ability of Lmo-InlA^m to breach the murine blood-placental barrier. Pregnant BALB/c mice were infected orally with 5×10^9 cfu of Lmo-EGD or Lmo-InlA^m at embryonic day (E13.5) or E14.5 of gestation. We find bacterial loads of fetal-placental units at day 2, 3, and 4 p.i. to be indistinguishable (Figure S5). Histopathological analysis of placentas and embryos confirm that lesions and inflammatory responses are similar in mice infected with either strain (Figure S6). Equivalent bacterial loads were also observed in fetal-placental units in female mice challenged with 5×10^4 cfu

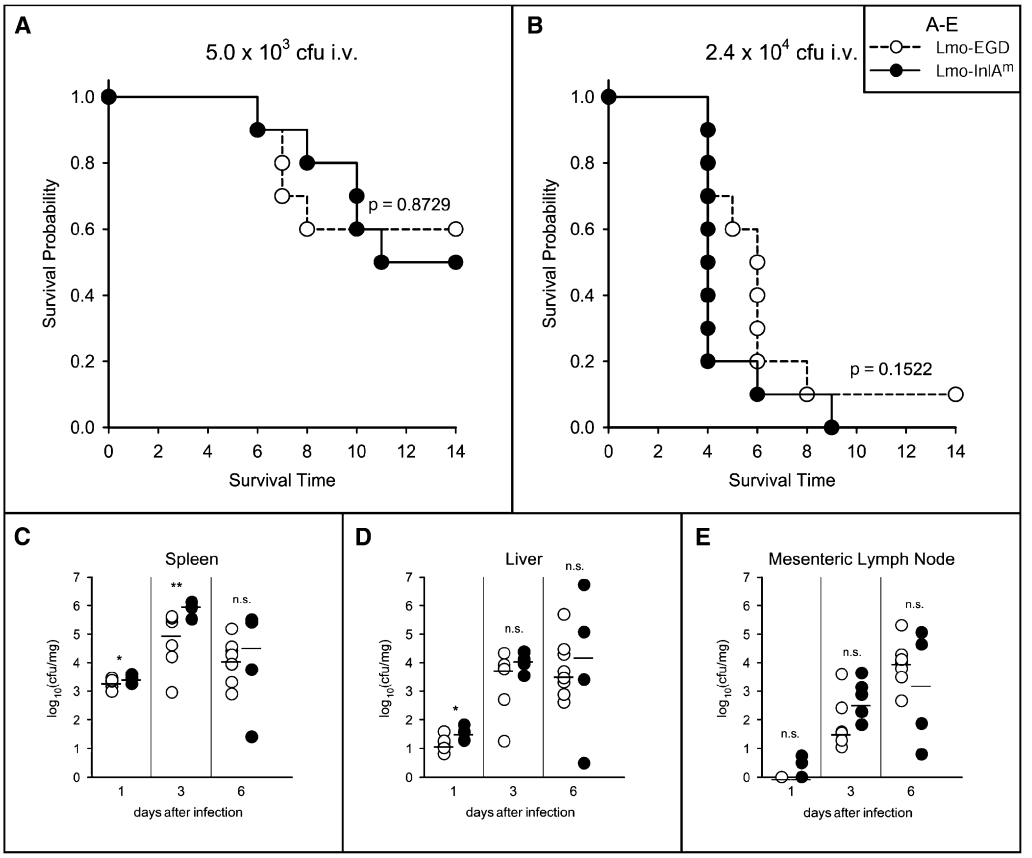

Figure 7. Survival Rates and Bacterial Organ Loads of Intravenously Infected Mice

Survival curves (A and B) and organ loads (C–E) of female C57BL/6J mice infected intravenously with either Lmo-EGD (dashed curves, ○) or Lmo-InlA^m (solid curves, ●). (A) and (B) show that the Lmo-InlA^m strain exhibits no significantly higher virulence compared to wild-type Lmo-EGD strain at low (5.0×10^3 cfu; [A]) and high (2.4×10^4 cfu; [B]) infection doses (n = 10). (C) and (D) show that both strains were inoculated i.v. with 9×10^3 bacteria for analyzing entry of bacteria in deeper tissues without crossing the intestinal barrier. Organ loads (n = 6) were analyzed at three different time points in the spleen (C), liver (D), and mesenteric lymph nodes (E). No appreciable enhanced virulence of the mutated strain Lmo-InlA^m could be detected. Note, however, that a statistically insignificant trend to higher virulence of Lmo-InlA^m is detectable in survival experiments, as well as in organ counts at days 3 and 6 p.i. Statistic evaluation is as shown in Figure 5.

Lmo-InlA^m and Lmo-EGD intravenously at day E14.5 (data not shown). Crossing of the blood-placental barrier is thus not InlA dependent in BALB/c mice.

DISCUSSION

Rationally Redesigning the InlA/hEC1 Complex

By using minimal, structure-derived modifications of a single pathogenicity factor, we have rationally redesigned the interface of InlA/hEC1 to increase its binding affinity and, in the process, modify the binding specificity of InlA to include murine E-cadherin. Incorporating these modifications into the original bacterium, we create a new listerial strain that mimics the uptake of wild-type Lmo-EGD in the human intestine in the mouse instead. Our approach circumvents the limitations of existing models of listeriosis in that both early and late responses are accessible and by uniquely providing a system in which both InlA and InlB are fully functional and expressed at wild-type levels. Because intestinal uptake depends only on murine E-cadherin, all mouse strains may be analyzed with Lmo-InlA^m. It should, furthermore, allow both host responses to food-borne pathogens crossing the intestinal barrier and the role of individual listerial factors during infection to be analyzed in an in vivo setting. To our knowledge, this is the first time that a virulence factor has been rationally modified, without relying on known mutations from related strains, or that a novel strain of a pathogen has been created with an extended host range.

Implications of InlA^m affinity for EC1

To induce uptake into epithelial cells by the zipper-mechanism, *L. monocytogenes* must adhere tightly to the eukaryotic-cell membrane. Accordingly, tighter adhesion of Lmo-InlA^m to Caco2 cells increases the efficiency of uptake compared to wild-type Lmo-EGD. Surprisingly,

however, the 6700-fold increased binding affinity merely causes a doubling in adhesion (Figure 3A). Because low binding affinity may be counteracted by high protein concentration, the efficient adhesion of Lmo-EGD to Caco2 cells is probably due to the high amount of E-cadherin on these cells.

In the intestinal epithelium, the amount of E-cadherin accessible to *L. monocytogenes* apically is limited because of its basolateral localization. The exception being multicellular junctions in epithelial monolayers where E-cadherin is transiently exposed (Pentecost et al., 2006). The low abundance of such junctions and the low affinity of InlA for its receptor E-cadherin would severely limit uptake of *L. monocytogenes* in vivo. By increase of binding affinity, the available E-cadherin could be utilized more efficiently, thus allowing a higher proportion of Lmo-InlA^m to invade the intestinal epithelium. Although pathogenicity would be increased, higher rates of uptake of InlA^m may prove to be advantageous therapeutically as in oral vaccination (Guimaraes et al., 2005), bacterial gene therapy (Dietrich et al., 1998), or drug delivery (Sleator and Hill, 2006). Because regulation of E-cadherin is, intimately linked to cell transformation and to the development of cancer (Wheelock and Johnson, 2003), InlA^m may, further, prove to be useful in the study of E-cadherin-mediated signal transduction.

InlA-Dependent and -Independent Routes of Listerial Infection

In mice, Lmo-EGD primarily target the Peyer's patches (Marco et al., 1997). Specialized, epithelial-like M cells (Clark and Hirst, 2002) covering these centers of mucosal immunity actively transport antigens and viable bacteria from the intestinal lumen to the underlying immune cells (Kraehenbuhl and Neutra, 2000). Food-borne pathogens such as *Salmonella* or *Shigella* exploit this indiscriminate uptake by reinvading M cells from the basolateral side, spreading to cells of the adjoining epithelium (Cossart and Sansonetti, 2004). E-cadherin on the basolateral side of M cells potentially allows Lmo-EGD to employ a similar strategy in humans. Our analyses, however, indicate that colonization of M cells and Peyer's patches by Lmo-InlA^m in mice is indistinguishable from that of Lmo-EGD. Reinfection of M cells is thus not part of the listerial invasion strategy. After their entry through Peyer's patches, both Lmo-EGD and Lmo-InlA^m are probably phagocytosed by macrophages independently of InlA and InlB. The macrophages then traffic to mesenteric lymph nodes and enter the blood stream as early as 12 hr p.i., thereby allowing bacteria to rapidly reach deeper tissues. Additionally, listerial dissemination to the spleen presumably involve CD8α^+ dendritic cells, again independent of InlA/B (Neuenhahn et al., 2006).

During this InlA-independent stage of listerial infection, Lmo-EGD does not colonize the intestinal epithelium. Mild immune responses in intestinal tissue in Lmo-EGD-infected mice after day 3 p.i. are possibly caused by immune cells activated in Peyer's patches migrating into the intestinal tissues (Mowat, 2003). Uptake of Lmo-EGD into subepithelial tissue is not triggered, thus allowing rapid remission.

Apart from Peyer's patches (InlA independent), Lmo-InlA^m additionally infects the intestinal epithelium (InlA dependent)—immunohistochemically observed 24 hr p.i. (Figure 6D). During the next 2 days, Lmo-InlA^m progressively infects subepithelial connective tissue documented by a steady increase in bacterial numbers in the intestine (Figure 5C). By day 3 p.i., large numbers of bacteria colonize the intestinal epithelial and subepithelial tissues (Figures 5C and 6L), thus opening a second, dominant route of listerial dissemination. Compared to the InlA-independent route, bacteria now access draining lymph nodes and blood, directly leading to a dramatic increase in bacterial numbers in the liver and spleen (Figure 5F). The heavy inflammation of the intestine additionally sequesters immune resources and weakens the host.

Increasing bacterial numbers in mesenteric lymph nodes and intestine until day 3 p.i. were also observed with a transgenic mouse model, although the effect is not as pronounced and subsides by day 5 p.i. (Lecuit et al., 2001).

The courses of infection after intravenous inoculation are, perhaps surprisingly, indistinguishable for the two listerial strains, implying that InlA is not essential for the later stages of listerial infections. Transport of *Listeria* by immune cells may be more important for systemic spreading than previously anticipated (Neuenhahn et al., 2006). A tendency of slightly higher virulence of Lmo-InlA^m indicates that InlA may nevertheless impart a slight advantage during this stage of the infection as well. Overall, InlA is crucial for establishing the infection of the intestinal epithelium. InlB and potentially other virulence factors then take over, leading to spread and systemic infection (Hamon et al., 2006).

L. monocytogenes Infection in Pregnant Mice

Pregnancy in humans increases susceptibility toward *L. monocytogenes* (Vazquez-Boland et al., 2001), and InlA is reportedly crucial in crossing the blood-placental barrier (Lecuit et al., 2004). Both pregnant mice (Le Monnier et al., 2006; Le Monnier et al., 2007) and guinea pigs (Bakardjiev et al., 2005) have been used to investigate this link. The usefulness of these models is, however, limited by the respective host specificities of InlA and InlB (see above). Lmo-InlA^m overcomes these limitations by providing active InlA and InlB for the murine system. Infecting pregnant mice orally with Lmo-InlA^m mimics the human course of infection and vertical transmission. We, however, do not observe a significant difference between Lmo-EGD and Lmo-InlA^m both by intravenous and oral infection of pregnant mice. This would indicate that the natural route of placental infection in mice is not dependent on either functional InlA or InlB. The uniquely invasive form of trophoblast-cell-mediated hemochorial placentation in humans (Moffett and Loke, 2006) could imply distinct susceptibilities for listerial infections. Alternatively, vertical transmission may occur by the "Trojan horse" strategy

via infected monocytes or macrophages as discussed for the blood-brain barrier (Drevets, 1999; Bakardjiev et al., 2005). In this case, InlA-mediated entry would play a subordinate role and would only be detectable in vitro or ex vivo where the "Trojan horse" mechanism is absent.

EXPERIMENTAL PROCEDURES

Protein Expression, Purification, and Crystallization

For structural and biophysical studies, functional fragments of InlA (residues 36–496) and E-cadherin (EC1, residues 1–105), were used. Murine EC1 (mEC1) was cloned from a cDNA library (German Resource Centre for Genome Research, clone ID IMAGp998A095392Q1) into the pGEX-6P-1 expression vector as previously described for hEC1 (Schubert et al., 2002). Site-directed mutations were introduced by QuikChange Mutagenesis (Stratagene). Proteins were expressed and purified as described (Schubert et al., 2002). Crystals were grown by vapor diffusion with 5 mg/ml of protein and a stoichiometric ratio of 1:1. The reservoir solution for InlA-variant/hEC1 crystals was 20%–25% PEG4000, 100 mM MES/Tris buffer (pH 7.0–7.5), 100 mM Na acetate, and 20–100 mM $CaCl_2$; for $InlA^{S192N-Y369S}$/mEC1, the reservoir solution was 20% PEG6000, 0.1 M Na citrate (pH 5.2), and 0.5 M LiCl, whereas 18% PEG400 (v/v) was added for cryoprotection.

Structure Determination

Data were collected at BL1, Protein Structure Factory, BESSY (λ = 0.95Å), and BW6, MPG ($InlA^{S192N}$/hEC1, λ = 1.05Å) with MARCCD detectors (Marresearch). Data were processed with XDS (Kabsch, 1988) and CCP4 suites (CCP4 [Collaborative Computational Project 4], 1994). The structure was solved by molecular replacement with EPMR (Kissinger et al., 1999). The structural model was built, analyzed, and validated with COOT (Emsley and Cowtan, 2004) and refined with REFMAC5 (Murshudov et al., 1997). Figures were prepared with PYMOL (www.pymol.org).

Isothermal Titration Calorimetry

Thermodynamic data were obtained with a MCS ITC (MicroCal). All samples were dialyzed against 50 mM HEPES (pH 7.5) and 20 mM $CaCl_2$, and 5–10 μl aliquots of InlA variants were injected into the ITC cell containing 1.35 ml of mEC1 or hEC1 variants, respectively. After correction for heat of dilution (ΔH_{dil}) data were analyzed with the "single set of independent sites" model (Micro Cal Origin 2.9).

Construction of the Isogenic Mutant Stain of *Listeria monocytogenes*

Full-length *inlA* was amplified from genomic DNA with the primers 5′-AGGAGGGATCCATGGTCGGACCAACGAGCCAACCGTG-3′ and 5′-AGGAGGCGGCCGCTGCTTGATTGGCGTTGGCACGGTG-3′ and cloned into the vector pPL2 (Lauer et al., 2002) with BamHI and NotI. We incorporated the desired mutations by excising a 1026 nucleotide BclI-BsaI fragment from pPL2 and replacing this with an equivalent fragment from a pGEX-6P-1 expression vector containing the mutation. A fragment, composed of the 3′-part of *inlA* and the 5′-part of *inlB* was amplified with primers 5′-AGGAGGGATCCAACCGTGACGC AGCCACTTAAGGC-3′ and 5′-AGGAGCAAGTCCTGCTAATGCTCTTA AATCGC-3′. Digesting this with BamHI and XbaI allowed its ligation into the BamHI/NheI-digested pETM11-GFP-FUS vector. The mutated 5′-part of *inlA* from the pPL2-$inlA^{S192N-Y369S}$ was cloned into vector pETM11-GFP-FUS-*inlAB* with restriction enzymes BamHI and AflII. The resulting plasmid bears full-length, mutated *inlA*, whereas the 5′ *inlB* fragment is fused to *gfp*. The $inlA^{S192N-Y369S}$-*inlB-gfp* fragment was excised from pETM11-GFP-FUS-$inlA^{S192N-Y369S}$-*inlB* by digesting with *Not*I, filling in by Klenow polymerase and dNTP (NEB), heat inactivation, and cutting with BamHI. The fragment was cloned into the pAUL-A shuttle vector (Chakraborty et al., 1992) cut with HindIII, filled in with Klenow polymerase and dNTP's, heat inactivated, and digested with BamHI. This vector pAUL-A-*inlA-inlB* was integrated (Chakraborty et al., 1992) into the *Listeria monocytogenes* EGD-e *inlA2* knockout strain (Lingnau et al., 1995). Reversion via homologous recombination was achieved as described (Lingnau et al., 1995). All steps were monitored by PCR analysis. The resulting strain, Lmo-$InlA^m$, carries the intact *inlAB* locus including two point mutations within *inlA*. The correct reversion was confirmed by PCR sequencing and immunoblotting with monoclonal antibodies against InlA and InlB.

Invasion Assays

Uptake of wild-type *Listeria monocytogenes EGD* serotype 1/2a (ATCC-number BAA-679) and Lmo-$InlA^m$ were analyzed with the human colorectal epithelial cell line Caco2 (ATCC HTB-37) and the murine macrophage-like cell line J774 (ATCC TIB-67). Caco2 cells were cultured in minimal essential medium (MEM) with Earle's salts (Invitrogen), supplemented with 20% FCS (PAA Laboratories), 2 mM glutamine, 1 mM sodium pyruvate, and 1% nonessential amino acids at 37°C/7% CO_2. J774 cells were cultured in Dulbecco's modified Eagle's medium (DMEM, Invitrogen) supplemented with 10% FCS (PAA Laboratories), and 2 mM glutamine at 37°C/7% CO_2. Two days prior to infection, 2×10^6 Caco2 cells or 2×10^5 J774 cells were seeded into 24-well plates. An overnight culture of *Listeria* was diluted 1:50 in BHI medium (Difco) and grown at 37°C till the middle of the log phase. Bacteria were washed twice in medium without FCS, and 8×10^6 (Caco2) or 2×10^5 (J774) bacteria were added to the monolayer (Caco2) or semiconfluent cells (J774)/well, centrifuged 5 min at 500 g, and incubated for 1 hr. Cells were washed with PBS. Medium containing 100 μg/ml gentamicin was added to kill extracellular bacteria. After 1, 2, 3, and 4 hr, cells were washed with PBS and lysed with sterile water containing 0.2% Triton X-100. Serial dilutions of cell lysates were plated onto BHI agar plates and incubated 24 hr at 37°C. Colonies were counted, and the recovery per well was determined. Each data point of one experiment was determined three times, and experiments were independently repeated in triplicate.

Adhesion assays were performed like invasion assays without centrifugation after addition of bacteria to Caco2 cells. Thirty minutes p.i., cells were washed 5-fold with PBS and lysed with 0.2% Triton X-100. Bacterial numbers were determined as described.

Mouse Infection

Ten-weeks-old female C57BL/6J mice were purchased from Harlan-Winkelmann (Borchen) and housed for a further week in the specific pathogen-free (SPF) animal facility (Helmholtz Centre for Infection Research) prior to infection. Lmo-EGD and Lmo-$InlA^m$ were grown in brain-heart infusion (BHI) broth (BD-Difco) until the end of the log-growth phase. After washing, bacteria were diluted in PBS. A total of 0.2 ml of the desired inoculum of either strain was mixed with 0.3 ml PBS containing 50 mg $CaCO_3$ (Lecuit et al., 2001). The suspension was inoculated intragastrically into mice (starved overnight, water allowed) with a 21 gauge feeding needle attached to a 1 ml syringe. Animals were then either monitored daily to determine survival rates or they were sacrificed and dissected for histological analysis or for determining bacterial counts in organs at the time points indicated. All animal experiments were reviewed and approved by local authorities. For infection of C57BL/6J mice intravenously, Lmo-EGD or Lmo-$InlA^m$ were prepared as described (Pasche et al., 2005). Survival rates and organ loads were determined as described for oral infections.

Infection of Pregnant Mice

BALB/c mice (Harlan-Winkelmann) were infected intragastrically or intravenously on day E13.5 or E14.5 as described above. Animals were examined daily. At indicated time points p.i., mice were sacrificed and the abdominal cavity was opened aseptically. Each placenta and fetus was independently dissected and analyzed with cfu determination or histopathology.

Bacterial Counts in Organs, Placentae, and Embryos

Stomach and small intestine were removed and incubated for 2 hr at 20°C in PBS supplemented with 100 μg/ml gentamicin (Gibco) to kill extracellular bacteria; other organs and embryos were sterilely dissected. Organs and embryos were homogenized, and serial dilutions were plated onto BHI agar, thus allowing a determination of bacterial counts per mg organ/embryo.

Statistical Analysis

Survival curves were statistically evaluated by Kaplan-Meier and Log-rank (Mantel-Cox) analyses. Bacterial loads are listed as median ±95% confidence intervals, statistically evaluated by the Mann-Whitney U nonparametic test. Calculations were done with GraphPadPrism4 (GraphPad Software). Differences were considered significant for $p \leq 0.05$.

Histology and Immunohistochemistry

Organs were fixed in 10% formalin, dehydrated, and embedded in paraffin. Sections of 5 μm were cut and stained with hematoxylin-eosin or used for immunohistochemistry (IHC). For detection of Lmo *Listeria*, O antiserum (Serotype 1 and 4; BD-Difco) was used. For detection, a secondary, peroxidase-coupled goat-anti-rabbit antibody was used. IHC sections were counterstained with hematoxylin.

Supplemental Data

Supplemental Data include six figures and one table and can be found with this article online at http://www.cell.com/cgi/content/full/129/5/891/DC1/.

ACKNOWLEDGMENTS

We thank our colleagues Daniela Gebauer and Stefanie Edler for excellent technical assistance and Dr. Theresia E.B. Stradal (Division of Cell Biology) for introducing T.W. to cell-biological methods and critical discussions. Funding by the Deutsche Forschungsgemeinschaft as part of the Priority Program 1150 (SCHU 1560/1-1 and 1-2) to W.D.S.; by the German National Genome Network (NGFN-2, 01GR0439) to A.L.; and by the Fonds der Chemischen Industrie to D.W.H is gratefully acknowledged. We thank the staffs of beam line BL1, Protein Structure Factory, BESSY (Berlin, Germany), and beam line BW6 (MPG DESY, Hamburg, Germany) for assistance and beam time.

Received: October 20, 2006
Revised: January 30, 2007
Accepted: March 15, 2007
Published: May 31, 2007

REFERENCES

Akira, S., Uematsu, S., and Takeuchi, O. (2006). Pathogen recognition and innate immunity. Cell *124*, 783–801.

Bakardjiev, A.I., Stacy, B.A., Fisher, S.J., and Portnoy, D.A. (2004). Listeriosis in the pregnant guinea pig: A model of vertical transmission. Infect. Immun. *72*, 489–497.

Bakardjiev, A.I., Stacy, B.A., and Portnoy, D.A. (2005). Growth of *Listeria monocytogenes* in the guinea pig placenta and role of cell-to-cell spread in fetal infection. J. Infect. Dis. *191*, 1889–1897.

Boneca, I.G., Dussurget, O., Cabanes, D., Nahori, M.A., Sousa, S., Lecuit, M., Psylinakis, E., Bouriotis, V., Hugot, J.P., Giovannini, M., et al. (2007). A critical role for peptidoglycan N-deacetylation in Listeria evasion from the host innate immune system. Proc. Natl. Acad. Sci. USA *104*, 997–1002.

CCP4 (Collaborative Computational Project 4) (1994). The CCP4 suite: Programs for protein crystallography. Acta Crystallogr D Biol Crystallogr *50*, 760–763.

Chakraborty, T., Leimeister-Wächter, M., Domann, E., Hartl, M., Goebel, W., Nichterlein, T., and Notermans, S. (1992). Coordinate regulation of virulence genes in *Listeria monocytogenes* requires the product of the *prfA* gene. J. Bacteriol. *174*, 568–574.

Clark, M.A., and Hirst, B.H. (2002). Expression of junction-associated proteins differentiates mouse intestinal M cells from enterocytes. Histochem. Cell Biol. *118*, 137–147.

Cossart, P., Pizarro-Cerda, J., and Lecuit, M. (2003). Invasion of mammalian cells by *Listeria monocytogenes*: Functional mimicry to subvert cellular functions. Trends Cell Biol. *13*, 23–31.

Cossart, P., and Sansonetti, P.J. (2004). Bacterial invasion: The paradigms of enteroinvasive pathogens. Science *304*, 242–248.

D'Souza-Schorey, C. (2005). Disassembling adherens junctions: Breaking up is hard to do. Trends Cell Biol. *15*, 19–26.

Dietrich, G., Bubert, A., Gentschev, I., Sokolovic, Z., Simm, A., Catic, A., Kaufmann, S.H., Hess, J., Szalay, A.A., and Goebel, W. (1998). Delivery of antigen-encoding plasmid DNA into the cytosol of macrophages by attenuated suicide *Listeria monocytogenes*. Nat. Biotechnol. *16*, 181–185.

Dramsi, S., Dehoux, P., Lebrun, M., Goossens, P.L., and Cossart, P. (1997). Identification of four new members of the internalin multigene family of *Listeria monocytogenes* EGD. Infect. Immun. *65*, 1615–1625.

Drevets, D.A. (1999). Dissemination of *Listeria monocytogenes* by infected phagocytes. Infect. Immun. *67*, 3512–3517.

Elsinghorst, E.A. (1994). Measurement of invasion by gentamicin resistance. Methods Enzymol. *236*, 405–420.

Emsley, P., and Cowtan, K. (2004). Coot: Model-building tools for molecular graphics. Acta Crystallogr D Biol Crystallogr. *60*, 2126–2132.

Gaillard, J.L., Berche, P., Frehel, C., Gouin, E., and Cossart, P. (1991). Entry of *L. monocytogenes* into cells is mediated by internalin, a repeat protein reminiscent of surface antigens from gram-positive cocci. Cell *65*, 1127–1141.

Gamblin, S.J., Haire, L.F., Russell, R.J., Stevens, D.J., Xiao, B., Ha, Y., Vasisht, N., Steinhauer, D.A., Daniels, R.S., Elliot, A., et al. (2004). The structure and receptor binding properties of the 1918 influenza hemagglutinin. Science *303*, 1838–1842.

Guimaraes, V.D., Gabriel, J.E., Lefevre, F., Cabanes, D., Gruss, A., Cossart, P., Azevedo, V., and Langella, P. (2005). Internalin-expressing *Lactococcus lactis* is able to invade small intestine of guinea pigs and deliver DNA into mammalian epithelial cells. Microbes Infect. *7*, 836–844.

Hamon, M., Bierne, H., and Cossart, P. (2006). *Listeria monocytogenes*: A multifaceted model. Nat Rev Microbiol. *4*, 423–434.

Heeney, J.L., Dalgleish, A.G., and Weiss, R.A. (2006). Origins of HIV and the evolution of resistance to AIDS. Science *313*, 462–466.

Kabsch, W. (1988). Evaluation of single-crystal X-ray diffraction data from a position-sensitive detector. J. Appl. Crystallogr. *21*, 916–924.

Khelef, N., Lecuit, M., Bierne, H., and Cossart, P. (2006). Species specificity of the *Listeria monocytogenes* InlB protein. Cell. Microbiol. *8*, 457–470.

Kissinger, C.R., Gehlhaar, D.K., and Fogel, D.B. (1999). Rapid automated molecular replacement by evolutionary search. Acta Crystallogr D Biol Crystallogr. *55*, 484–491.

Kraehenbuhl, J.P., and Neutra, M.R. (2000). Epithelial M cells: Differentiation and function. Annu. Rev. Cell Dev. Biol. *16*, 301–332.

Lauer, P., Chow, M.Y., Loessner, M.J., Portnoy, D.A., and Calendar, R. (2002). Construction, characterization, and use of two *Listeria monocytogenes* site-specific phage integration vectors. J. Bacteriol. *184*, 4177–4186.

Le Monnier, A., Join-Lambert, O.F., Jaubert, F., Berche, P., and Kayal, S. (2006). Invasion of the placenta during murine listeriosis. Infect. Immun. *74*, 663–672.

Le Monnier, A., Autret, N., Join-Lambert, O.F., Jaubert, F., Charbit, A., Berche, P., and Kayal, S. (2007). ActA is required for crossing of the fetoplacental barrier by *Listeria monocytogenes*. Infect. Immun. *75*, 950–957.

Lecuit, M., Dramsi, S., Gottardi, C., Fedor-Chaiken, M., Gumbiner, B., and Cossart, P. (1999). A single amino acid in E-cadherin responsible for host specificity towards the human pathogen *Listeria monocytogenes*. EMBO J. *18*, 3956–3963.

Lecuit, M., Vandormael-Pournin, S., Lefort, J., Huerre, M., Gounon, P., Dupuy, C., Babinet, C., and Cossart, P. (2001). A transgenic model for listeriosis: role of internalin in crossing the intestinal barrier. Science *292*, 1722–1725.

Lecuit, M., and Cossart, P. (2002). Genetically-modified-animal models for human infections: The Listeria paradigm. Trends Mol. Med. *8*, 537–542.

Lecuit, M., Nelson, D.M., Smith, S.D., Khun, H., Huerre, M., Vacher-Lavenu, M.C., Gordon, J.I., and Cossart, P. (2004). Targeting and crossing of the human maternofetal barrier by *Listeria monocytogenes*: Role of internalin interaction with trophoblast E-cadherin. Proc. Natl. Acad. Sci. USA *101*, 6152–6157.

Lecuit, M. (2005). Understanding how *Listeria monocytogenes* targets and crosses host barriers. Clin. Microbiol. Infect. *11*, 430–436.

Lewis, D.B. (2006). Avian flu to human influenza. Annu. Rev. Med. *57*, 139–154.

Li, F., Li, W., Farzan, M., and Harrison, S.C. (2005). Structure of SARS coronavirus spike receptor-binding domain complexed with receptor. Science *309*, 1864–1868.

Lingnau, A., Domann, E., Hudel, M., Bock, M., Nichterlein, T., Wehland, J., and Chakraborty, T. (1995). Expression of the *Listeria monocytogenes* EGD *inlA* and *inlB* genes, whose products mediate bacterial entry into tissue culture cell lines, by PrfA-dependent and -independent mechanisms. Infect. Immun. *63*, 3896–3903.

Marco, A.J., Altimira, J., Prats, N., Lopez, S., Dominguez, L., Domingo, M., and Briones, V. (1997). Penetration of *Listeria monocytogenes* in mice infected by the oral route. Microb. Pathog. *23*, 255–263.

Mengaud, J., Ohayon, H., Gounon, P., Mege, R.-M., and Cossart, P. (1996). E-cadherin is the receptor for internalin, a surface protein required for entry of *L. monocytogenes* into epithelial cells. Cell *84*, 923–932.

Moffett, A., and Loke, C. (2006). Immunology of placentation in eutherian mammals. Nat. Rev. Immunol. *6*, 584–594.

Mowat, A.M. (2003). Anatomical basis of tolerance and immunity to intestinal antigens. Nat. Rev. Immunol. *3*, 331–341.

Murshudov, G.N., Vagin, A.A., and Dodson, E.J. (1997). Refinement of macromolecular structures by the maximum-likelihood method. Acta Crystallogr D Biol Crystallogr. *53*, 240–255.

Neuenhahn, M., Kerksiek, K.M., Nauerth, M., Suhre, M.H., Schiemann, M., Gebhardt, F.E., Stemberger, C., Panthel, K., Schröder, S., Chakraborty, T., et al. (2006). CD8α^+ dendritic cells are required for efficient entry of *Listeria monocytogenes* into the spleen. Immunity *25*, 619–630.

Pasche, B., Kalaydjiev, S., Franz, T.J., Kremmer, E., Gailus-Durner, V., Fuchs, H., Hrabe de Angelis, M., Lengeling, A., and Busch, D.H. (2005). Sex-dependent susceptibility to *Listeria monocytogenes* infection is mediated by differential interleukin-10 production. Infect. Immun. *73*, 5952–5960.

Pentecost, M., Otto, G., Theriot, J.A., and Amieva, M.R. (2006). *Listeria monocytogenes* invades the epithelial junctions at sites of cell extrusion. PLoS Pathog. *2*, e3.

Sabet, C., Lecuit, M., Cabanes, D., Cossart, P., and Bierne, H. (2005). LPXTG protein InlJ, a newly identified internalin involved in *Listeria monocytogenes* virulence. Infect. Immun. *73*, 6912–6922.

Schubert, W.D., Urbanke, C., Ziehm, T., Beier, V., Machner, M.P., Domann, E., Wehland, J., Chakraborty, T., and Heinz, D.W. (2002). Structure of internalin, a major invasion protein of *Listeria monocytogenes*, in complex with its human receptor E-cadherin. Cell *111*, 825–836.

Shen, Y., Naujokas, M., Park, M., and Ireton, K. (2000). InlB-dependent internalization of *Listeria* is mediated by the Met receptor tyrosine kinase. Cell *103*, 501–510.

Sleator, R.D., and Hill, C. (2006). Patho-biotechnology: Using bad bugs to do good things. Curr. Opin. Biotechnol. *17*, 211–216.

Stevens, J., Blixt, O., Tumpey, T.M., Taubenberger, J.K., Paulson, J.C., and Wilson, I.A. (2006). Structure and receptor specificity of the hemagglutinin from an H5N1 influenza virus. Science *312*, 404–410.

Vazquez-Boland, J.A., Kuhn, M., Berche, P., Chakraborty, T., Dominguez-Bernal, G., Goebel, W., Gonzalez-Zorn, B., Wehland, J., and Kreft, J. (2001). Listeria pathogenesis and molecular virulence determinants. Clin. Microbiol. Rev. *14*, 584–640.

Weiss, R.A. (2003). Cross-species infections. Curr. Top. Microbiol. Immunol. *278*, 47–71.

Wheelock, M.J., and Johnson, K.R. (2003). Cadherins as modulators of cellular phenotype. Annu. Rev. Cell Dev. Biol. *19*, 207–235.

Yap, G.S., and Sher, A. (2002). The use of germ line-mutated mice in understanding host-pathogen interactions. Cell. Microbiol. *4*, 627–634.

Accession Numbers

Crystallographic data have been deposited with the Protein Data Bank (accession numbers 2OMV, 2OMW, and 2OMY).